CuNPs/RGO/cotton fabric electrode for flexible high-performance supercapacitors

Xingyu Jiang[1] , Bing Bai[1], Jiaxin Shui[1], Linlin Qiu[1], and Pingfan Du[1,*]

[1]*College of Textile Science and Engineering, Zhejiang Sci-Tech University, Hangzhou 310018, People's Republic of China*

ABSTRACT

A fabric electrode with a 3D structure consisting of copper nanoparticles (CuNPs), reduced graphene oxide (RGO), and cotton was fabricated by a simple, efficient, environmentally friendly, and low-cost method. With cotton fabric as the textile base, RGO provides double electric layer capacitors, which also can help connect the cotton fibers in series, making the cotton fabric a high-speed conductive channel. Additionally, the CuNPs provide pseudocapacitance and storage space for ions. This three-dimensional synergistic effect in the fabric electrode led to a specific capacitance of 197.4 F g^{-1} and a good charge–discharge performance. The assembled all-solid symmetric supercapacitor showed a specific capacitance of 179.4 F g^{-1}, with a maximum energy density of 8.52 Wh kg^{-1} and power density of 100.05 W kg^{-1}. The cheap and readily available raw materials make this fabric-based electrode easy to manufacture on a large scale, making it a promising candidate for wearable devices.

1 Introduction

With the recent development of flexible wearable energy storage devices, improving their performance has become an important area of research. Traditional energy storage devices typically have a large volume and are rigid, making them unsuitable for wearable applications. Flexible supercapacitors have a high power density, long cycle life, excellent charge–discharge capacity, and reliable safety, making them ideal for wearable devices [1, 2]. A flexible and lightweight electrode is the key to the excellent performance of supercapacitors. At present, many common flexible materials, such as fibers [3], fabrics [4], metal sheets [5], and films [6], have been used as supports for flexible electrodes.

Cotton is a cellulose polymer, with fibrous binary sugar repeating units in its structure. Among the various natural fibers, cotton is the most popular due to its softness, breathability, and comfort [7], making it an ideal choice for a fabric electrode substrate. Supercapacitors can be classified into three broad categories: double-layer capacitors (EDLCs), pseudocapacitors, and hybrid capacitors [8]. EDLCs store charge electrostatically; thus, their properties mainly depend on the surface properties of the material. Carbon-based materials with high specific surface area, such as graphene [9], carbon nanotubes [10], and carbon fibers [11], are usually selected as

Address correspondence to E-mail: dupf@zstu.edu.cn

electrode materials for EDLCs. Pseudocapacitors store charge through reversible redox reactions on the surface of electrically active substances.

Both types of capacitors have certain unique advantages and disadvantages. Currently, the focus is on improving the energy density and reducing the cost of supercapacitors without sacrificing high output power and excellent cycle stability. Researchers attempt to combine pseudocapacitive materials (such as metals or metal compounds and conductive polymers) with conductive carbon-based materials to develop a hierarchical multilayer structure to obtain improved storage performance and power density of the electrode, without reducing the conductivity of the electrode.

Graphene is a two-dimensional carbon nanomaterial with the thickness of a single atom layer, formed by combining carbon atoms in the sp^2 hybrid mode. Graphene has numerous unique properties, such as high surface area, high electrical conductivity, and excellent mechanical, thermal, and electrical stability [12]. In recent years, graphene has been widely used as an electrode material for supercapacitors. Hybrid electrodes prepared by combining graphene with pseudocapacitor materials have also shown enhanced electrochemical performance in experiments over a period of time. Karami et al. used a simple electroless silver plating (ESP) method to fabricate Ag/RGO/CF (cotton) fabric electrodes with a layered structure, which exhibited excellent cycling stability and a high specific capacitance of 426 F g^{-1} [13]. Kim et al. fabricated a high-performance hybrid fabric electrode by spraying a mixture of SnO_2 and RGO onto a textile substrate by supersonic spraying; the device showed both long service life and high specific capacitance [14]. Studies have shown that combining carbon-based materials and metal pseudocapacitors may be a good choice. Even in other uses of electrode also can improve the overall performance [15, 16]. However, the high cost of raw materials and technology makes mass production and large-scale application of these electrodes a luxury.

In this study, we proposed a Cu/RGO/CF multilayer composite electrode prepared by simple in situ polymerization. First, silk screen printing was used to coat CF with graphene oxide (GO) and $Na_2S_2O_4$ solution was used to reduce GO to reduced GO (RGO), which is simple, efficient, environmentally friendly, and repeatable. Subsequently, copper nanoparticles (CuNPs) were generated on the RGO/

CF surface by in situ polymerization, which required a simple water bath and ultrasonication instead of complex and costly processes. Except for hydrazine hydrate, all the materials used are environmentally friendly. Moreover, graphene's ability to adsorb heavy metal ions has been proven and applied [17, 18], therefore, adding graphene into fabric electrode can effectively reduce the pollution diffusion caused by fabric electrode during use. Copper, which is one of the most common metals and has excellent electrical conductivity, was used to construct a Cu–RGO–CF multilayer structure, with the stacking of CuNPs on the electrode surface, providing additional storage properties. The morphology, structure, and electrochemical performance of the electrode were evaluated.

2 Experimental

2.1 Materials

Graphite powder (325 mesh) was purchased from Jiangsu XFNANO Technology Co., Ltd. Potassium permanganate and acetone were purchased from Zhejiang Hannuo Chemical Technology Co., Ltd. Lithium chloride, PVA 1799, copper sulfate pentahydrate, ammonia, polyvinylpyrrolidone (PVP), and ethylene diamine tetraacetic acid (EDTA) were bought from Shanghai Macklin Biochemical Co., Ltd. 80% hydrazine hydrate and 30% hydrogen peroxide were purchased from Shanghai Lingfeng Chemical Reagent Co., Ltd. Sulfuric acid and 37% hydrochloric acid were purchased from Hangzhou Shuanglin Chemical Reagent Co. Ltd. Sodium nitrate was purchased from Tianjin Bodi Chemical Co., Ltd. Sodium disulfite was purchased from Wuxi Zhanwang Chemical Reagent Co. Ltd. Potassium hydroxide was purchased from Hangzhou Gaojing Chemical Co. Ltd. Combed CFs, for textile specifications, were purchased from the local fabric market in Shaoxing, Zhejiang Province.

2.2 Synthesis of GO

GO was synthesized by the modified Hummers method. 120 ml of 98% sulfuric acid and 2 g of sodium nitrate were added to a glass beaker, stirred at a constant speed for 15 min. Then, 4 g of natural flake graphite was added and stirred at 200 rpm for

30 min. Then, 16 g of potassium permanganate powder was slowly added to the reaction system. The temperature was kept below 5 °C during the whole process. After potassium permanganate was fully integrated into the reaction system, the reaction system was maintained at 40 °C for 10 h and stirred during this time. After that, 200 ml of iced deionized water was slowly added. Then, 8-ml hydrogen peroxide was added slowly until the whole system turned golden brown. Finally, the reactants were washed three times with 10% dilute hydrochloric acid and the mixture was allowed to settle completely. The supernatant was drained and the lower sediments were filled into a dialysis bag of 8000–14,000 MW and rinsed with deionized water for 1–2 weeks until the pH was close to 7. The GO in the dialysis bag was removed and sonicated for 1 h at room temperature, encapsulated, and stored for later use.

2.3 Preparation of RGO/CF

CF was cut into pieces and soaked in a mixture of acetone and ethanol (volume of acetone and ethanol = 1:3). By ultrasonic washing 1 h at room temperature, the GO solution was prepared to a concentration of 30 mg ml^{-1}, and the surface of CF was uniformly coated with GO by screen printing, with a mesh aperture of 100 mesh. The fabric we got for this part is called GCF. The GCF was dried in an oven and then the sample was immersed in Na_2SO_4 solution at a concentration of 100 mM and maintained at 85 °C for 6 h until the GO on the fabric surface was reduced to RGO. The samples were rinsed repeatedly with deionized water and dried in the oven. The silk screen-printed CFs, with RGO, are referred to as RCF.

2.4 Preparation of Cu/RGO/CF electrode

The fabric electrodes were prepared by growing CuNPs on the surface of RCF by in situ polymerization [19, 20]. 100 ml of 0.5-mol copper sulfate solution was prepared, and ammonia was slowly added to it until the pH of solution reached 11. Additionally, 3 g of EDTA was added as the complexing agent and 2 g of PVP was used as the dispersant. The solution was stirred until completely dissolved and referred to as solution (A). A hydrazine hydrate solution was used as a reducing agent. 50 ml of 1.5-mol l^{-1} hydrazine

hydrate solution was prepared and referred to as solution (B). RCF was immersed in solution A for 10 min. Then, solution B was added to solution A in a water bath at 60 °C under ultrasonication and allowed to react for 15 min. The samples were rinsed repeatedly with deionized water to remove any unfairly bound CuNPs. The samples were dried at 80 °C, placed in a vacuum oven, and kept at 80 °C for 8 h to solidify. The prepared sample is referred to as CRCF (Fig. 1).

2.5 Characterization of electrochemical properties

The electrochemical properties of the prepared fabric electrodes were characterized by cyclic voltammetry (CV), electrochemical impedance (EIS), and constant current charge and discharge (GCD). The prepared fabric electrode was cut into rectangular samples (1 × 2 cm). The CV and EIS tests were performed with a three-electrode system. The system was tested with RCF and CRCF as working electrodes, platinum sheet electrode as the counter electrode, Ag/AgCl as the reference electrode, and 1 M KOH solution as the electrolyte. The tests were performed on a Zahner Electrochemical workstation (manufactured by Zahner, Germany). The constant current charge and discharge test (GCD) was carried out with a double-electrode system. Two identical RCF electrodes or CRCF electrodes were used as the positive and negative poles of the supercapacitor, with LiCl/PVA gel as the electrolyte [21]. The test was carried out on the Land Electric battery test system (manufactured by Wuhan Land Electric Electronics Co., Ltd.). The fabric electrodes were assembled into sandwich-type supercapacitors and tested.

CV curves of the RCF and CRCF fabric electrodes were recorded at different scanning rates (5, 10, 20, 30, 50 mV s^{-1}) in a potential window of − 0.2 V to − 0.8 V (vs. Ag/AgCl) in 1-M KOH electrolyte. The specific capacitance of the fabric electrode is calculated based on Eq. (1):

$$C_s = \frac{A}{M \cdot k \cdot \Delta v},\tag{1}$$

where C_s is the specific capacitance (F g^{-1}), A is the area of the CV curve, M is the load mass of the active substance (g), k is the scanning rate (V s^{-1}), and Δv is the range of working potential (V) [22].
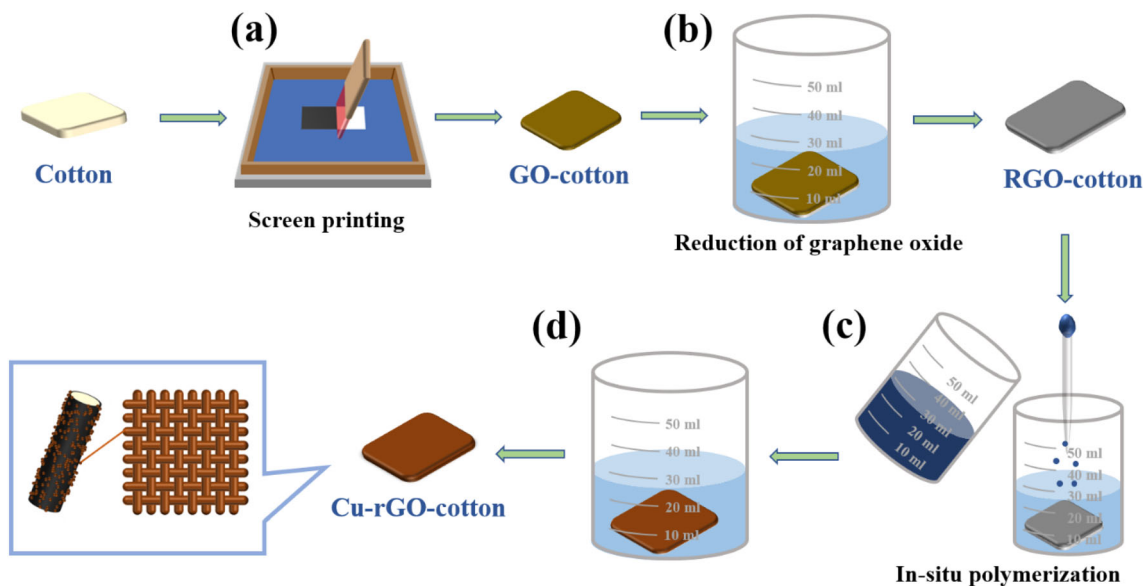
Fig. 1 Process of fabricating the fabric electrode: (a) Silk screen printing of the graphene oxide on CF. (b) Sample placed in $Na_2S_2O_4$ solution for 6 h at 85 °C to reduce GO. (c) At 60 °C and under ultrasonication, hydrazine water was added to the copper ammonia solution. (d) CuNPs were deposited on the fabric surface by in situ polymerization

The EIS test was performed at AC amplitudes of 5 mV and at frequencies ranging from 100 kHz to 10 mHz. The GCD recorded the cycle stability of supercapacitors assembled by RCF and CRCF. The charging and discharging performance of the fabric capacitors was tested under different circuit densities. The specific capacitance is calculated based on Eq. (2) and the GCD curve.

$$C_s = \frac{I \cdot \Delta t}{M \cdot \Delta v'}, \quad (2)$$

where I is the discharge current (A), Δt is the discharge time (s), M is the load mass of the active substance (g), and $\Delta v'$ is the discharge voltage interval of the discharge process after removing the voltage drop [23].

In addition, the energy density and power density of the capacitor were calculated based on the GCD curve and Eqs. 3–4, which were used to analyze the performance of the battery:

$$E = \frac{C_s \cdot \Delta v'^2}{7.2}, \quad (3)$$

$$P = \frac{E \times 3600}{\Delta t}, \quad (4)$$

where E is the energy density (Wh kg^{-1}) and P is the power density (W kg^{-1}) [24].

3 Results and discussion

3.1 Surface morphology of the fabric electrode

The morphology of the fabric electrode was characterized by SEM, as shown in Fig. 2. Figure 2a and b shows the untreated CF, where the surface is smooth and clean and micron-sized cotton fiber is visible, indicating that a porous structure with hierarchical properties was obtained. Figure 2c and d shows the fabric morphology after screen printing of GO. The surface layer of the cotton fiber was completely covered by GO, and the gap between the fibers was filled by GO lamellae. As shown in Fig. 2e and f, the reduced fabric structure was not damaged by the chemical reduction, and the GO covered by the fiber surface was completely reduced to RGO, which confirmed the stable deposition of graphene nanosheets on the surface of CF. The graphene lamellae connect the cotton fibers, forming a network with high conductivity and electrical activity on the surface of the CF; the wavy pattern of RGO on the CF was visible. Figure 2g and h shows the final shape of the fabric electrode. The fabric surface was completely covered by an elemental Cu layer. The size of CuNPs varied from tens of nanometers to hundreds of nanometers. Pores were formed by the accumulation of metal particles on the graphene sheet, and the
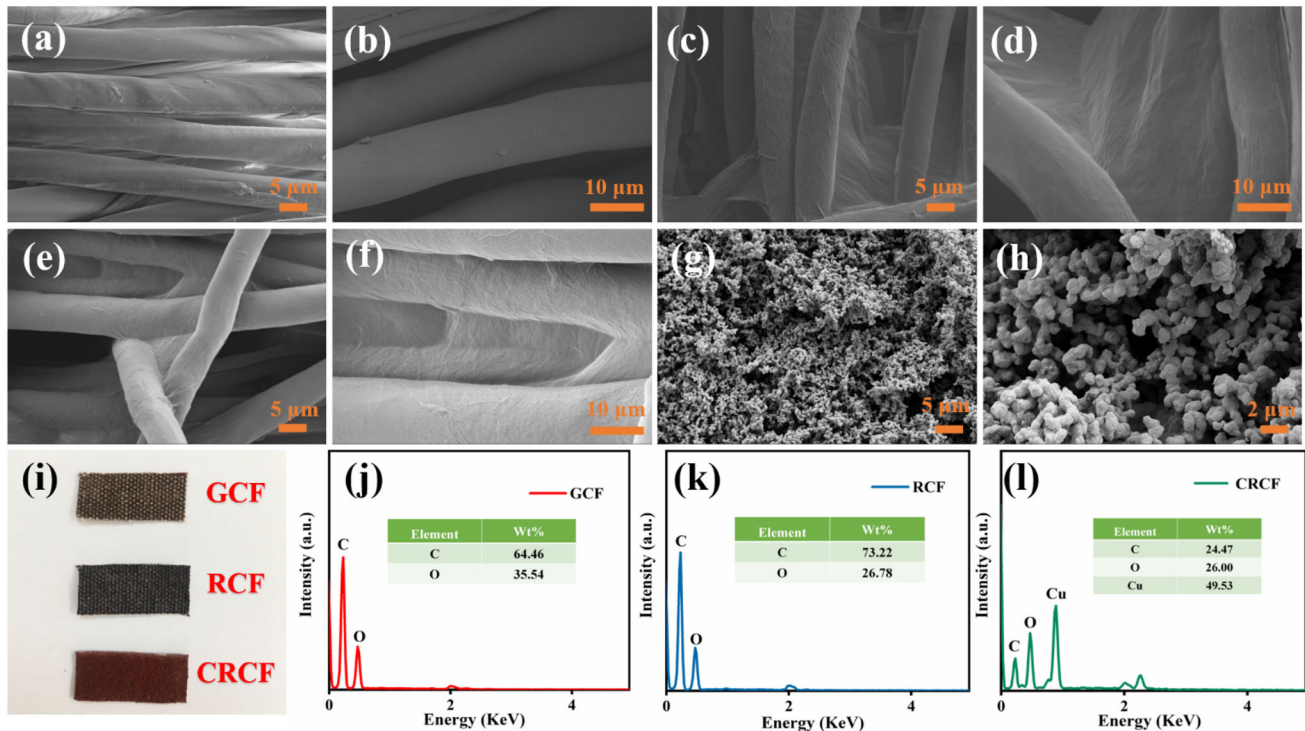
Fig. 2 SEM images of CF (**a**, **b**), GCF (**c**, **d**), RCF (**e**, **f**), and CRCF (**g**, **h**). **i** Physical photos of GCF, RCF, and CRCF. EDS spectra for GCF (**j**), RCF (**k**), and CRCF (**l**)

three-dimensional structure of Cu–RGO–CF was obtained. During the experiment, the sample was immersed in the mixed system of solutions A and B. Hydrazine hydrate in solution B acts as a strong reducing agent, which can reduce copper ions in solution A to copper metal (as shown in Eq. 5) and deposit it on the sample; the deposited copper is typically homogeneous in size and compact [25, 26].

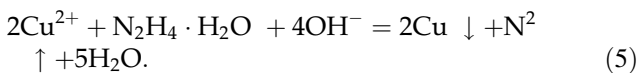$$2Cu^{2+} + N_2H_4 \cdot H_2O + 4OH^- = 2Cu \downarrow + N^2 \uparrow + 5H_2O. \tag{5}$$

Figure 2i shows the photos of GCF, RCF, and CRCF. EDS analysis was used to measure the element content of samples at different stages. Figure 2j shows the EDS diagram of GCF, with C and O elements in the samples. After chemical reduction, Fig. 2k shows the EDS diagram of RCF. It can be found that the proportion of O element in the sample is reduced because the oxygen-containing functional group of GO is destroyed during chemical reduction, and it is constantly reduced to RGO. Figure 2i shows the EDS diagram of CRCF. The adhesion of CuNPs resulted in the highest specific gravity of Cu element on the fabric surface, indicating that the in situ

polymerization effect was excellent and the generated CuNPs could be well attached to the fabric surface.

3.2 XRD analysis of fabric electrode surface

Samples from each step of the fabric electrode preparation were analyzed by X-ray diffraction. As shown in Fig. 3a, in the XRD pattern of the original pure CF, peaks at 17.4°, 22.9°, and 25.7° are the characteristic peaks of the crystal structure of cellulose I [27]. These peaks were also found in the XRD spectra of the GF and RF fabrics, indicating that the crystal structure of CFs was not affected during the subsequent screen printing and chemical reduction processes. However, the diffraction peaks associated with GO and RGO were missing in the GCF and RCF profiles. The XRD patterns of GO and RGO are shown in Fig. 3b and c, with characteristic peaks around 9.8° and 23.5° [28], respectively, since the relative diffraction peak is obscured by the CF diffraction peak [29]. For the CRCF electrode, diffraction peaks appeared at 43.7°, 50.9°, and 74.5°, which is consistent with the XRD standard pattern of
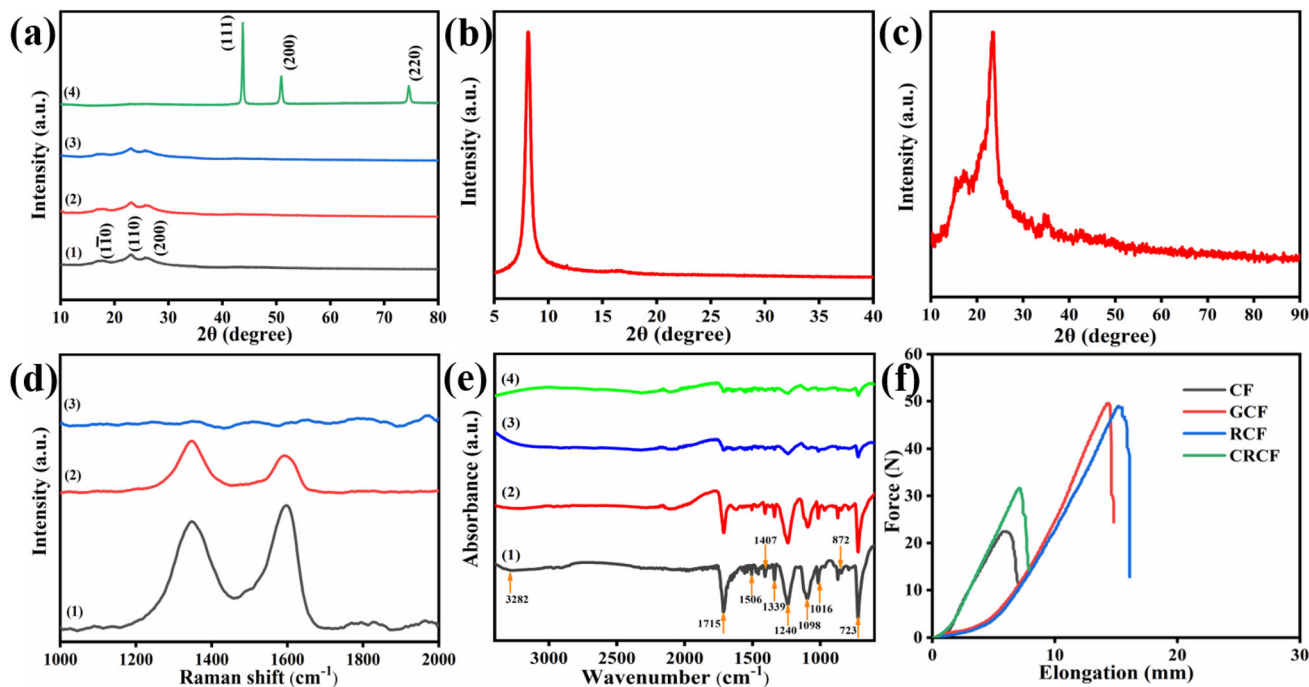
Fig. 3 **a** XRD patterns of samples from each fabrication step: (1) CF, (2) GCF, (3) RCF, and (4) CRCF. **b** XRD patterns of **b** GO and **c** RGO. **d** Raman spectra at different fabrication stages: (1) GCF, (2) RCF, and (3) CRCF. **e** ATR–FTIR spectra at different stages of fabrication: (1) CF, (2) GCF, (3) RCF, and (4) CRCF. **f** Fracture elongation curve of each morphology during fabrication

Cu in the cubic crystal system (No. 04-0836), indicating that the product was elemental Cu [30]. No other diffraction peak was obtained, indicating that the electrode surface was completely covered by elemental Cu.

3.3   Surface Raman analysis of fabric electrode

Samples from each step were characterized by Raman spectroscopy. Figure 3d shows two significant peaks in the fabric after screen printing GO and chemical reduction. After the chemical reduction, the defects in the original samples will be improved, which can significantly decrease the D peak intensity and increase the peak intensity ratio I_d/I_g from 0.91 to 1.40. Thus, most of the oxygen-containing functional groups on the GO lamella were removed during the reduction process and a good graphene layer formed on the surface of the CF, leading to high conductivity, also proving the success of reduction [31]. However, in situ polymerization led to the formation of CuNPs, which completely covered the graphene layer; thus, the D and G peaks on the sample surface disappeared. Since there were no

carbon atoms at the top surface of the fabric, the characteristic peaks could not be detected, which demonstrated the success of the pseudocapacitance loading.

3.4   ATR–FTIR spectroscopy of fabric electrodes

The samples from each stage of the fabric electrode fabrication were analyzed by infrared spectroscopy, as shown in Fig. 3e. The absorption peak of untreated CF at 3100–3300 cm^{-1} corresponds to the stretching vibration of O–H [13]. The stretching vibration peak of C–O was observed at 1715 cm^{-1} [32]. The weak peaks at 1407 and 1339 cm^{-1} can be attributed to the bending vibration of the C–H plane or the skeleton vibration of the C–C single bond. The absorption peaks at 1240 and 1098 cm^{-1} are associated with the stretching vibration peaks of C–O in the epoxy group, and peaks at 872 and 723 cm^{-1} belong to the bending vibration outside the C–H plane [33]. In the infrared spectrum of the reduced samples, the peak intensities of nearly all the oxygen-containing functional groups were weakened, indicating that GO had been successfully reduced to RGO. In the infrared spectrum of

CRCF, no additional peaks were detected because the fabric surface was covered by Cu.

3.5 Mechanical properties of fabric electrodes

The mechanical properties of fabric electrodes are important for achieving good service life and wearable performance. Samples from each stage of the electrode fabrication were cut into 5 × 3 (cm) strips and tested for maximum tensile strength. As shown in Fig. 3f, after screen printing GO on CF, the mechanical strength of the fabric improved significantly, since the GO nanosheets were attached to the CF surface, and their interaction enhanced the friction between the fibers [34]. The tensile strength of the fabric electrode decreased significantly after the attachment of CuNPs. Since CF is alkali resistant, however, in this experiment, CF immersed in a solution system with PH value of about 11 is out of its adaptive range, which reduces its fiber endurance to a certain extent. Even so, the mechanical strength of CRCF is significantly higher than that of the original CF fabric, which meets the mechanical requirements of wearable fabrics.

3.6 Supercapacitive properties of fabric electrodes

Figure 4a shows the CV curves of the RCF fabric and CRCF fabric electrodes at a sweep speed of 5 mV s^{-1} in 1-M KOH solution. The curve of the RCF electrode is different from the rectangle of the standard double-layer capacitor, which is associated with two main reasons, described as follows. The RCF electrode resistance is large, leading to a reduced current density. In addition, according to literature, RGO in an alkaline electrolyte can be referred to as a hybrid electrode [35]. Therefore, the deviation of the CV curve of the RCF fabric, from the rectangular shape, is partly attributed to the pseudocapacitance generated by the electrode as a mixed electrode in 1-M KOH electrolyte. The CV curve of the CRCF fabric electrode shows an obvious pseudocapacitance behavior, with a significant redox peak. However, the lack of complete symmetry indicates poor reversibility of CRCF in the electrode system, which is also a common drawback of pseudocapacitance [36]. In CRCF, while the surface of RGO is completely covered by CuNPs and it does not show any EDLC

behavior, RGO still plays an important role. The uniform dispersion of RGO on the surface of CF fills the gap between fibers, making CF a high-speed channel for ion diffusion. Then, CuNPs could attach to the surface of RGO with the appropriate morphology, particle size, and density. The three-dimensional structure makes the ions in the electrolyte diffuse rapidly and significantly enhances the energy storage performance of the electrode. The specific capacitance of the CRCF fabric reached 197.4 F g^{-1}, which was 5.2 times higher than that of the RCF fabric (37.9 F g^{-1}). The higher specific capacitance of the CRCF fabric can be attributed to the synergistic effect between CuNPs and RGO.

Figure 4b shows the CV curves of the CRCF fabric electrode at different scanning rates. The contour of the curve gradually deviates from the original shape, with the increase in the scanning rate. This is due to the difference in the rate of ion migration from the electrolyte to the electrode/electrolyte interface and from the electrode/electrolyte interface to the fabric electrode surface. As a result, ions pile up at the interface, which polarizes the electrode [33, 37, 38].

Figure 4c shows the decrease in the specific capacitance of the CRCF fabric as the scanning rate increases. The trend of reducing specific capacitance is associated with the inability of the ions in the electrolyte to diffuse to the electrode, as observed with most reported fabric or fabric-like supercapacitors. However, the specific capacitance was still several times higher than that of the RCF fabric, which demonstrates its excellent capacitance.

Electrochemical impedance measurements were used to obtain the electrode resistance and ion diffusion coefficient. Figure 4d shows the Nyquist diagram of the RCF fabric. The half-arc in the high-frequency region corresponds to the charge transfer process, and the resistance of the RCF electrode is about 90–120 Ω. The slope corresponding to the low-frequency region continues to decrease, indicating poor ion diffusion. Thus, the electrode response and ion transport in fabric electrodes need further improvement.

Figure 4e shows the Nyquist plot of the CRCF fabric. The resistance of the fabric electrode decreased to single digits after being covered with CuNPs. Additionally, the rate of ion diffusion in the system significantly increased, corresponding to an increase in the slope of the low-frequency phase [39]. Due to
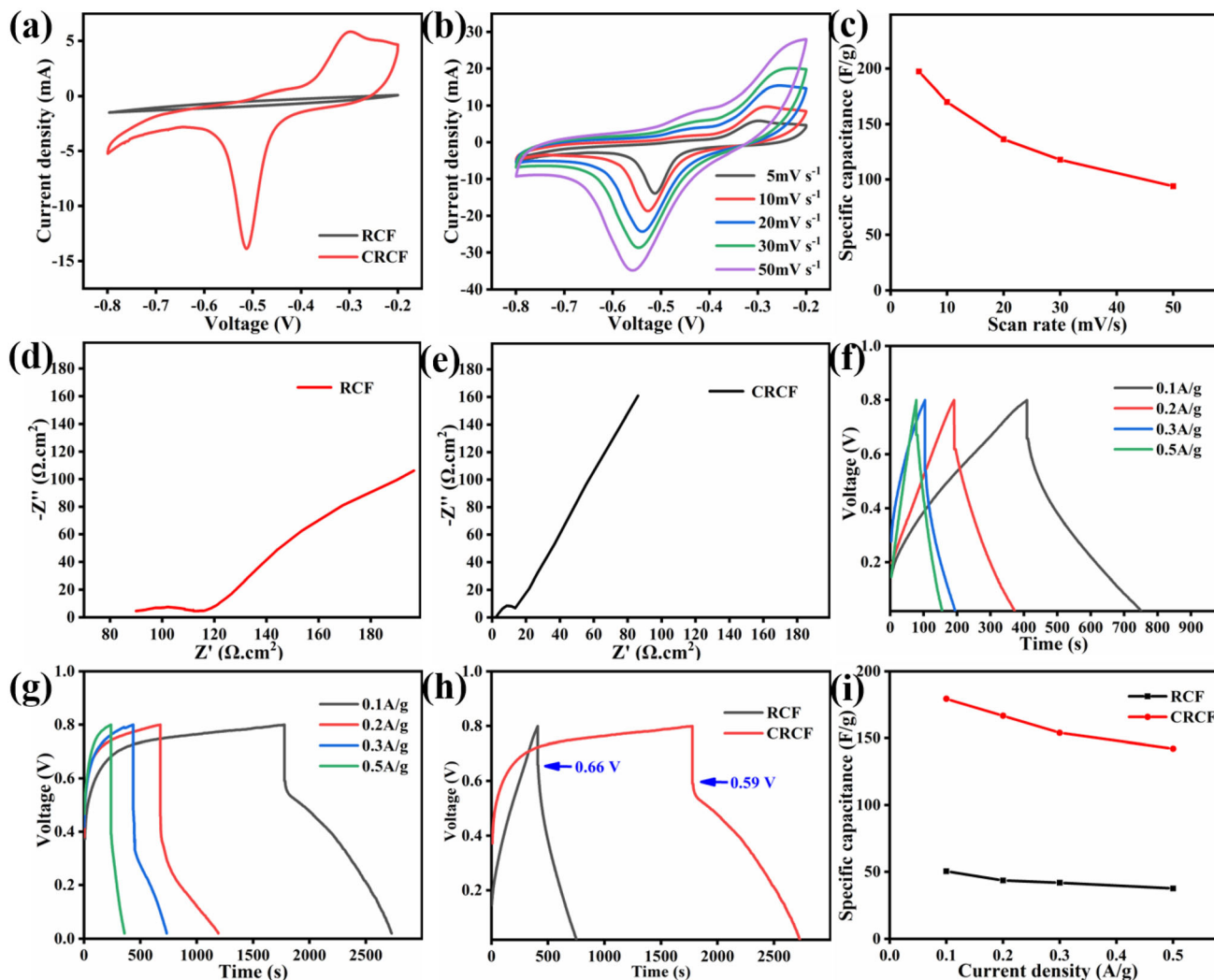
Fig. 4 (a) Comparison of the CV curves of the RCF and CRCF electrodes at 5 mV s^{-1}. **b** CV curves of the CRCF electrodes at different scanning rates. **c** Changes in the specific capacitance of the CRCF electrodes at different scanning rates. **d** Nyquist plot of the RCF electrode and **e** CRCF electrode. **f** GCD curve of the RCFSCs and **g** CRCFSCs at different current densities. **h** Comparison of the GCD curves of RCFSC and CRCFSC at 0.1 A g^{-1}. **i** Changes in the specific capacitance of RCFSCs and CRCFSCs at different current densities

the existence of the CuNP layer, its electrical conductivity and electrochemical properties significantly increased. Meanwhile, CRCF has smaller semicircle diameter in the high-frequency region than RCF, indicating lower charge transfer resistance (R_{ct}) [40].

The GCD test was used to evaluate the electrochemical performance of supercapacitors (SCs). Figure 4f and g shows the GCD curves of the SCs assembled with RCF and CRCF at a current density of 0.1 A g^{-1}, respectively. Figure 4h shows the comparison of the GCD curves of RCFSC and CRCFSC at 0.1 A g^{-1}. RCFSCs benefit from the better stability of EDLC and have a more symmetrical GCD curve [41].

However, CRCFSCs have a longer discharge time and specific capacitance and their discharge performance is better than that of RCF under any current density gradient ratio. When the current density was 0.1 A g^{-1}, the maximum specific capacitance of CRCFSC (179.4 F g^{-1}) was 3.6 times that of RCFSC (50.5 F g^{-1}). As shown in Fig. 4i, when the current density increased from 0.1 to 0.5 A g^{-1}, the specific capacitance of the CRCF-based SCs decreased to 142.2 F g^{-1}, which only attenuated by 21%, demonstrating a good rate performance [42]. However, since metallic Cu is highly reactive, the reversibility of the pseudocapacitance reaction was not strong, and the
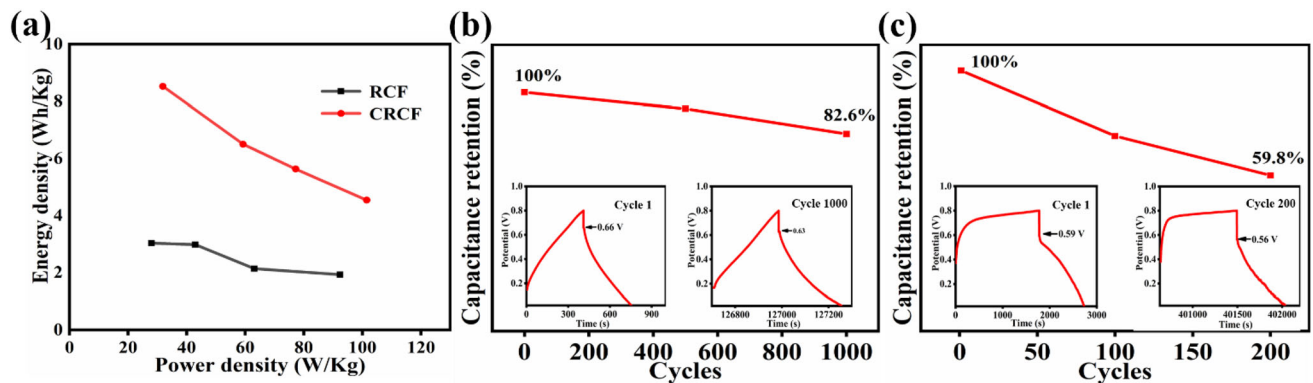
Fig. 5 **a** Ragone plot of RCFSCs and CRCFSCs. **b** Capacitance retention rate of RCFSCs for 1000 cycles. **c** Capacitance retention rate of CRCFSCs for 200 cycles

GCD curve of the CRCFSC showed a large voltage drop, impacting the efficiency of the assembled supercapacitor.

The energy density and power density of the fabric capacitor were calculated and the corresponding Ragone Plot is shown in Fig. 5a. The maximum energy density of CRCFSC was 8.52 Wh kg^{-1}, and the power density was 100.05 W kg^{-1}. These values are normal [43, 44]. Considering the influence of the large voltage drop, the energy storage performance of CRCFSC was still excellent. Moreover, the comprehensive performance of CRCFSC was much higher than that of RCFSC, which is also associated with the attachment of metal pseudocapacitors.

Cycling stability is an important criterion for evaluating the service life of supercapacitors. Figure 5b and c shows the capacitance retention of RCFSCs and CRCFSCs after multiple charges and discharges. As mentioned above, RCFSCs exhibited stability common to EDLCs, with a capacitance retention rate of 82.6% after 1000 cycles. The stability of CRCFSCs was lower than that of the CRCFSCs; after 200 cycles, the capacitance retention rate was 59.8%. This is because Cu has high activity as a metal pseudocapacitor. Although Cu reacts slowly with the ambient air and moisture, the efficiency of the reaction tends to intensify when the current is switched on. Additionally, the formation of a blue–green solid at the junction of electrolyte and electrode was observed during cycling, which is attributed to the reaction of CuNPs to form basic copper carbonate. Thus, as cycling continues, the effective active substance in the supercapacitor gradually reduces,

reducing the specific capacitance and reversibility, which is another aspect that requires further study.

4 Conclusion

In this study, a flexible, solid-state, fully symmetrical textile cotton-based supercapacitor was prepared. The fabrication of the fabric-based electrode was simple, i.e., by screen printing and in situ polymerization, which is environmentally friendly and involves low-cost raw materials. The assembled supercapacitor showed a good specific capacitance and charge–discharge performance, The specific capacitance of CRCF fabric electrode reached 197.4 F g^{-1}, and the supercapacitor prepared based on the fabric electrode was 179.4 F g^{-1}, the maximum energy density was 8.52 Wh kg^{-1}, and the power density was 100.05 W kg^{-1}. However, the stability and rate performance of fabric electrode need to be further improved. To sum up, the fabric electrode prepared in this experiment is ready for mass production and has great potential in smart textiles and wearables.

Author contributions

of the manuscript were performed by LLQ. PFD contributed to supervision, project administration, writing, reviewing, and editing of the manuscript, and funding acquisition. All authors read and approved the final manuscript.

Funding

Data availability

All data included in this study are available upon request by contact with the corresponding author.

Declarations

Conflict of interest The authors declare that they have no known competing financial interest or personal relationships that could have appeared to influence the work reported in this paper.

References

1. V. Rajendran, A.M. Mohan, M. Jayaraman, T. Nakagawa, All-printed, interdigitated, freestanding serpentine interconnects based flexible solid state supercapacitor for self-powered wearable electronics. Nano Energy **65**, 1 (2019)

2. C.J. Raj, R. Manikandan, W. Cho, K.H. Yu, B.C. Kim, High-performance flexible and wearable planar supercapacitor of manganese dioxide nanoflowers on carbon fiber cloth. Ceram. Int. **46**, 21736 (2020)

3. W.J. Ma, S.H. Chen, S.Y. Yang, W.P. Chen, W. Wang, Y.H. Cheng, M.F. Zhu, Flexible all-solid-state asymmetric supercapacitor based on transition metal oxide nanorods/reduced graphene oxide hybrid fibers with high energy density. Carbon **113**, 151 (2017)

4. M.Y. Zhou, H.H. Zhang, Y. Qiao, C.M. Li, Z.S. Lu, A flexible sandwich-structured supercapacitor with poly(vinyl alcohol)/H_3PO_4-soaked cotton fabric as solid electrolyte, separator and supporting layer. Cellulose **25**, 3459 (2018)

5. Q.Y. Huang, L.B. Liu, D.R. Wang, J.J. Liu, Z.F. Huang, Z.J. Zheng, One-step electrospinning of carbon nanowebs on metallic textiles for high-capacitance supercapacitor fabrics. J. Mater. Chem. A **4**, 6802 (2016)

6. D. Park, S. Selvam, J. Yim, Conformable on-skin supercapacitor-integrated, strain sensor based on multioxidant-functionalized thermoplastic polyurethane/reduced graphene oxide/polypyrrole composite films. N. J. Chem. **46**, 10535 (2022)

7. Z.W. Sun, X.F. Wang, Z.W. Liu, Q.S. Gu, Y. Zhang, Z.K. Li, H.F. Ke, J. Yang, J.H. Wu, L.Q. Wu, G.Y. Zhang, C.Y. Zhang, Z.Y. Ma, Genome-wide association study discovered genetic variation and candidate genes of fibre quality traits in *Gossypium hirsutum* L. Plant Biotechnol. J. **8**, 982 (2017)

8. S. Najib, E. Erdem, Current progress achieved in novel materials for supercapacitor electrodes: mini review. Nanoscale Adv. **1**, 2817 (2019)

9. Y.B. Tan, J. Lee, Graphene for supercapacitor applications. J. Mater. Chem. A **1**, 14814 (2013)

10. J. Ren, L. Li, C. Chen, X.L. Chen, Z.B. Cai, L.B. Qiu, Y.G. Wang, X.R. Zhu, H.S. Peng, twisting Carbon Nanotube fibers for both wire-shaped Micro-Supercapacitor and Micro-Battery. Adv. Mater. **25**, 1155 (2013)

11. J. Noh, C.M. Yoon, Y.K. Kim, J. Jang, High performance asymmetric supercapacitor twisted from carbon fiber/MnO_2 and carbon fiber/MoO_3. Carbon **116**, 470 (2017)

12. Y. Wang, S.S. Li, H.Y. Yang, J. Luo, Progress in the functional modification of graphene/graphene oxide: a review. RCS Adv. **10**, 15328 (2020)

13. Z. Karami, M. Youssefi, K. Raeissi, M. Zhiani, An efficient textile-based electrode utilizing silver nanoparticles/reduced graphene oxide/cotton fabric composite for high-performance wearable supercapacitors. Electrochim. Acta **20**, 1 (2020)

14. T. Kim, E.P. Samuel, C. Park, Y. Kim, A. Aldalbahi, F. Alotaibi, S.S. Yoon, Wearable fabric supercapacitors using supersonically sprayed reduced graphene and tin oxide. J. Alloys Compd. **856**, 157902 (2021)

15. G. Bharath, A. Hai, K. Rambabu, F. Ahmed, A.S. Haidyrah, N. Ahmad, S.W. Hasan, F. Banat, Hybrid capacitive deionization of NaCl and toxic heavy metal ions using Faradic electrodes of silver nanospheres decorated pomegranate peel-derived activated carbon. Environ. Res. **197**, 111110 (2021)

16. G. Bharath, K. Rambabu, F. Banat, A. Hai, A.F. Arangadi, N. Ponpandian, Enhanced electrochemical performances of peanut shell derived activated carbon and its Fe_3O_4 nanocomposites for capacitive deionization of Cr(VI) ions. Sci. Total Environ. **691**, 713 (2019)

17. G. Bharath, K. Rambabu, C. Aubry, M.A. Haija, A.K. Nadda, N. Ponpandian, F. Banat, Self-assembled Co_3O_4 nanospheres on N-Doped reduced Graphene Oxide (Co_3O_4/N-RGO) Bifunctional Electrocatalysts for Cathodic reduction of CO_2

and anodic oxidation of Organic Pollutants. ACS Appl. Energy Mater. **4**, 11408 (2021)

18. G. Bharath, A. Hai, K. Rambabu, D. Savariraj, Y. Ibrahim, F. Banat, The fabrication of activated carbon and metal-carbide 2D framework-based asymmetric electrodes for the capacitive deionization of Cr(VI) ions toward industrial wastewater remediation. Environ. Sci. Water Res. Technol. **6**, 351 (2020)

19. F. Ran, Y.T. Tan, W.J. Dong, Z. Liu, L.B. Kong, L. Kang, In situ polymerization and reduction to fabricate gold nanoparticle-incorporated polyaniline as supercapacitor electrode materials. Polym. Adv. Technol. **29**(6), 1697-1705 (2018)

20. V. Vijayakumar, B. Anothumakkool, S. Kurungot, M. Winter, J.R. Nair, In situ polymerization process: an essential design tool for lithium polymer batteries. Energy Environ. Sci. **14**, 2708 (2021)

21. X.Y. Xie, B.J. Xin, Z.M. Chen, Y.Q. Xu, Preparation and characterization of PANI-PPY/PET fabric conductive composite for supercapacitors. J. Text. Inst. **11**, 2443 (2021)

22. A.I. Oje, A.A. Ogwu, M. Mirzaeian, N. Tsendzughul, A.M. Oje, Pseudo-capacitance of silver oxide thin film electrodes in ionic liquid for electrochemical energy application. J. Sci. Adv. Mater. Devices **4**, 213 (2018)

23. X.T. Xu, Y. Liu, M. Wang, C. Zhu, T. Lu, R. Zhao, L.K. Pan, Hierarchical hybrids with microporous carbon spheres decorated three-dimensional graphene frameworks for capacitive applications in supercapacitor and deionization. Electrochim. Acta **193**, 88 (2016)

24. W.W. Liu, X.B. Yan, J.W. Lang, C. Peng, Q. Xue, Flexible and conductive nanocomposite electrode based on graphene sheets and cotton cloth for supercapacitor. J. Mater. Chem. **22**, 17245 (2012)

25. N. Sreeju, A. Rufus, D. Philip, Microwave-assisted rapid synthesis of copper nanoparticles with exceptional stability and their multifaceted applications. J. Mol. Liq. 221, 1008-1021 (2016)

26. A. Khan, A. Rashid, R. Younas, R. Chong, A chemical reduction approach to the synthesis of copper nanoparticles. Nano Lett. **6**, 21 (2016)

27. Z. Tang, W.Y. Li, X.X. Lin, H. Xiao, Q.X. Miao, L.L. Huang, L.H. Chen, H. Wu, TEMPO-Oxidized cellulose with high degree of Oxidation. Polymers **9**, 421 (2017)

28. S. Jadhav, R.S. Kalubarme, C. Terashima, B.B. Kale, V. Goadbole, Manganese dioxide/reduced graphene oxide composite an electrode material for high-performance solid state supercapacitor. Electrochim. Acta **299**, 34 (2019)

29. G.Q. Xie, J. Cheng, Y.F. Li, P.X. Xi, F.J. Chen, H.Y. Liu, F.P. Hou, Y.J. Shi, L. Huang, Z.H. Xu, D.C. Bai, Z.Z. Zeng, Fluorescent graphene oxide composites synthesis and its biocompatibility study. J. Mater. Chem. **22**, 9308 (2012)

30. X.R. He, Y.L. Hu, H.Q. Tian, Z.P. Li, P. Huang, J. Jiang, C. Wang, In situ growth of flexible 3D hollow tubular Cu_2S nanorods on Cu foam for high electrochemical performance supercapacitor. J. Materiomics **6**, 192 (2020)

31. J. Li, C.L. Chen, R. Zhang, X.K. Wang, Nanoscale Zero-Valent Iron particles supported on reduced Graphene Oxides by using a plasma technique and their application for removal of heavy-metal ions. Chem. Asian J. **10**, 1410 (2015)

32. Y.Z. Li, Y.F. Zhang, H.R. Zhang, T.L. Xing, G.Q. Chen, A facile approach to prepare a flexible sandwich structured supercapacitor with rGO-coated cotton fabric as electrodes. RSC Adv. **9**, 4180 (2019)

33. M. Barakzehi, M. Montazer, F. Sharif, T. Norby, A. Chatzitakis, A textile-based wearable supercapacitor using reduced graphene oxide/polypyrrole composite. Electrochim. Acta **305**, 187 (2019)

34. J.S. Cui, S.X. Zhou, Highly conductive and ultra-durable electronic textiles via covalent immobilization of carbon nanomaterials on cotton fabric. J. Mater. Chem. C **6**, 12273 (2018)

35. Y.J. Oh, J.J. Yoo, Y.I. Kim, J.K. Yoon, H.N. Yoon, J.H. Kim, S.B. Park, Oxygen functional groups and electrochemical capacitive behavior of incompletely reduced graphene oxides as a thin-film electrode of supercapacitor. Electrochim. Acta **116**, 118 (2014)

36. X.L. Deng, Z.X. Wei, C.Y. Cui, Q.H. Liu, C.Y. Wang, J.M. Ma, Oxygen-deficient anatase $TiO_2@C$ nanospindles with pseudocapacitive contribution for enhancing lithium storage. J. Mater. Chem. A **10**, 1 (2018)

37. B. Pandit, V.S. Devika, R.S. Babasaheb, Electroless-deposited Ag nanoparticles for highly stable energy-efficient electrochemical supercapacitor. J. Alloys Compd. **17**, 1 (2017)

38. Y.L. Shao, M.F. El-Kady, J.Y. Sun, Y.J. Li, Q.H. Zhang, M.F. Zhu, H.Z. Wang, B. Dunn, R.B. Kaner, Design and mechanisms of asymmetric supercapacitors. Chem. Rev. **118**, 9233 (2018)

39. Q. Chen, Y. Hu, C.G. Hu, H.H. Cheng, Z.P. Zhang, B.H. Shao, L.T. Qu, Graphene quantum dots–three-dimensional graphene composites for high-performance supercapacitors. Phys. Chem. Chem. Phys. **16**, 19307 (2014)

40. L.M. Chen, H.Y. Yu, Z.H. Li, X. Chen, W.L. Zhou, Cellulose nanofiber derived carbon aerogel with 3D multiscale pore architecture for high performance supercapacitors. Nanoscale **13**, 17837 (2021)

41. J.H. Yu, F.F. Xie, Z.C. Wu, T. Huang, J.F. Wu, D.D. Yan, C.Q. Huang, L. Li, Flexible metallic fabric supercapacitor based on graphene/polyaniline composites. Electrochim. Acta **259**, 968 (2018)

42. D.J. Ahirrao, A.K. Pal, V. Singh, N. Jha, Nanostructured porous polyaniline (PANI) coated carbon cloth (CC) as

electrodes for flexible supercapacitor device. J. Mater. Sci. Technol. **88**, 168 (2021)

43. S. Mao, Z.H. Wen, B. Zheng, J.B. Chang, X.K. Huang, J.H. Chen, Hierarchical nanohybrids with porous CNT-Networks decorated crumpled Graphene Balls for Supercapacitors. ACS Appl. Mater. Interfaces **6**, 9881 (2014)

44. C. Wang, K. Hu, W.J. Li, H.Y. Wang, H. Li, Y. Zou, C.C. Zhao, Z. Li, M. Yu, P.C. Tan, Z. Li, Wearable wire-shaped symmetric supercapacitors based on activated Carbon-Coated Graphite fibers. ACS Appl. Mater. Interfaces **10**, 34302 (2018)